Journal of ETA Maritime Science 2024;12(2):199-212

Calculation of Time-Independent Maneuvering Coefficients of an Underwater Vehicle Based on Single Grid Structure

Oğuzhan Kırıkbaş, Şakir Bal

İstanbul Technical University, Faculty of Naval Architecture and Ocean Engineering, İstanbul, Türkiye

Abstract

A simulation approach relying on a single grid topology has been employed to replicate the motion characteristics of different experimental facilities, including towing tank, rotating arm mechanism, and planar motion mechanism using a single mesh. The control volume and computational mesh setup was built in a way to enable to perform both steady and time dependent simulations to compute entire set of coefficients required by the standard submarine equations of motion. Mesh is consisted of a rectangular prism shaped background and a spherical overset domain which can be rotated, circulated and oscillated depending on the simulation type. To enable the implementation of this approach to the rotating arm simulations, modifications to source code of the open-source computational fluid dynamics software OpenFOAM have been made. Motivation is to change the perspective on the problem by using the knowledge of mathematics behind the solution algorithms and the software structure. In this study extensive set of time-independent coefficients obtained via straight and oblique towing as well as steady rotation simulations are presented for a fully appended generic submarine geometry. Results are then compared with the benchmark experimental data. It is found that the consistency between results are quite satisfactory.

Keywords: DARPA Suboff, Maneuvering coefficient, Rotating arm, OpenFOAM

1. Introduction

Maneuvering for underwater vehicles (UVs) refers to the controlled and intentional alteration of the vehicle's position, orientation or trajectory in a fluid medium. This process involves the precise modulation of hydrodynamic forces and moments in 6-DoF and achieved through the deflection of control surfaces and/or propulsor rotation rate as well as ballast intake or discharge. The prerequisite for solving the maneuvering problem is the expression of these complex motion behavior via a mathematical model known as a maneuvering model. Maneuvering coefficients serve as essential parameters in a maneuvering model, quantifying hydrodynamic forces and moments acting on an UV during various maneuvers. Initially developed by Gertler and Hagen [1], a generalized UV maneuvering model based on the motion equations has undergone revisions by Feldman [2] incorporating crossflow terms.

These coefficients can be roughly categorized based on the time dependency of the computational fluid dynamics (CFD) simulation used in their calculations. Time-independent maneuvering coefficients are fundamental parameters that impact various aspects of UV design, operation, and safety. Their accurate determination contributes to the overall effectiveness and reliability of UVs in a wide range of applications including dynamic stability and control system effectiveness.

Despite recent proposals for more comprehensive approaches to the maneuvering problem of UVs, based on the "synthetic" motion [3] or free running of UV [4-9]; literature commonly employs CFD simulations mimicking experimental setups. A towing tank is imitated in CFD environment as rectangular prism control volume for straight and oblique towing simulations. Whereas rotating arm (RA) mechanism is imitated as a circular segment shaped control volume for mimicking the steady rotational motion. The main difference between CFD simulations and experiments in terms of motion is the object/medium exposed to this motion. For the sake of computational efficiency; the body is

Address for Correspondence: Oğuzhan Kırıkbaş, İstanbul Technical University, Faculty of Naval Architecture and Ocean Engineering, İstanbul, Türkiye
E-mail: kirikbas17@itu.edu.tr
ORCID ID: orcid.org/0000-0002-2504-8727

Received: 26.01.2024
Last Revision Received: 20.04.2024
Accepted: 24.04.2024

To cite this article: O. Kırıkbaş, and Ş. Bal, "Calculation of Time-Independent Maneuvering Coefficients of an Underwater Vehicle Based on Single Grid Structure." *Journal of ETA Maritime Science*, vol. 12(2), pp. 199-212, 2024

at rest and the flow is passing through the body in the CFD simulations of both cases. In order to achieve this for RA simulations and expose the fluid domain to additional forces arose from rotation, governing equations of the flow must be modified. Planar motion mechanism (PMM) simulations are unsteady in nature due to involving the motion of the body with respect to fluid medium as in the experiments.

Unsteady numerical simulations adhere to the availability of high amount of computational resources. Additionally they are subject to certain numerical limitations (i.e. Courant-Friedrichs-Lewy or CFL condition) which strongly effects the potential improvement in their accuracy level with the available computational power. On contrary to the other types of facilities, PMM experiments/simulations can attain an extensive set of coefficients. However their results cannot be used directly to obtain relevant hydrodynamic coefficients. Fourier transform is required for the frequency-time domain transition of the data.

Since motions created by a PMM are time-dependent in nature, PMM simulations are only feasible after achieving adequate computational capacity [10,11]. Phillips et al. [12], Zhang et al. [13] and Pan et al. [14] are among the pioneers in this category. Besides sufficiently accurate methods have been proposed since the beginning of the last century for the UV like shapes [15-18]. As a result of this; researchers initially focused their attention on time independent coefficients.

There's a strong background in understanding oblique flows and cross-flow separation on axisymmetric bodies. Together with the low demand of computational resources and ease of implementation of the problem setup to the CFD environment, working on linear damping coefficients became the initial area of research. Toxopeus [19] investigated the local field variables as well as global measures of the flow around a non-appended submarine hull at incidence.

Motion stability both in horizontal and vertical plane is expressed in terms of stability indices (i.e. G_v and G_h). Ensuring the vehicle has desired level of course-keeping stability in both planes rotational motion coefficients must also be calculated along with the linear damping coefficients. Phillips et al. [20] used time-independent CFD simulations to predict the dynamic stability margin of an autonomous UV by calculating the required coefficients.

Inherently these coefficients are also related with the steady (third phase) turning motion and they can be computed rather than actual rotation of the vehicle with respect to mesh but modification of the flow field to expose UV to Coriolis force and centrifugal acceleration. This is known as multiple rotating reference frame (MRF) approach or frozen rotor method due to its primary are of application is turbomachinery. Although MRF introduce a certain amount of error, the accuracy of the results are generally adequate for an engineering solution.

Common feature of the above mentioned studies is the use of different control volume shapes for mimicking the different experimental facilities. A small number of studies have devised techniques to consolidate different domain types into a single one, enabling the performance of multiple types of analyses. Oblique towing and steady turning simulations are performed by Cao et al. [21] using a single computational domain. They adopt SRF approach to reflect the effects of rotation on the governing equations of the flow.

Differently from [21]; Xiaocui et al. [22] employ MRF approach in a spherical mesh zone located inside a background cuboid control volume. The center of rotation is transferred from the pivot point of the RA mechanism to the body-fixed coordinate system origin. In order to achieve this the authors modified source codes of the CFD software with a user defined function. The source term that represents the Coriolis force and centrifugal acceleration in momentum equation was manipulated. By doing this, using same control volume for both oblique towing and RA simulations becomes possible. In general, these studies demonstrated the adequacy and efficiency of the steady state assumption when solid body motion does not involve. Together with the added mass coefficients, this time-independent coefficients can be used in a maneuvering model to perform trajectory calculations. In terms of definitive maneuvers the trajectories associated with maneuvers steady in nature such as turning circle is essentially governed by time-independent coefficients.

Utilizing the methodology proposed in [10] and [11], the control volume and computational mesh setup used in this study was built in a way to enable to perform both steady (i.e oblique towing and RA) and time independent simulations. By doing so it is possible to compute almost all of the coefficients required by the standard submarine equations of motion [2]. Preliminary results which are limited with the linear damping coefficients presented in [10] and [11] enlarged in this study. An extensive set of hydrodynamic coefficients in relation to time-independent analyses including control surface coefficients are given at this time to show the effectiveness of the single grid topology approach. Independent variable (i.e. drift/attack/control surface deflection angle and rotation radius) intervals, which corresponds to the linear and non-linear variations of dependent variables (i.e. force and moments) are investigated. Results are benchmarked with the RA experiments of Zhao et al. [23,24], PMM experiments of Roddy [25] and wind tunnel experiments of Khan et al. [26] where relevant. This paper organized as follows. Section 2 describes the governing equations including the modifications, as well as the coordinate system, UV geometry, domain, mesh and boundary conditions. Simulation matrix

is given at the end of this section. The computational mesh is validated and the numerical results are given in Section 3. The final remarks are presented in the conclusion section.

2. Materials and Methods

2.1. Geometry and Main Particulars

The model used in the CFD simulations is the fully-appended DARPA Suboff submarine (AFF-8). UV geometry in 3D is depicted in Figure 1. The main particulars of the model were defined in [27] and are provided in Table 1.

2.2. Coordinate System and Standard Convention

The body fixed coordinate system and standard direction convention for forces and moments as well as control surface (rudder and elevator) deflections are shown in Figure 2. Surge, sway and heave forces are identified as X, Y, and Z and the roll, pitch and yaw moments as K, M and N respectively. Prime (') symbol is employed to indicate dimensionless quantities and nondimensionalization is made according to Equations (1) and (2).

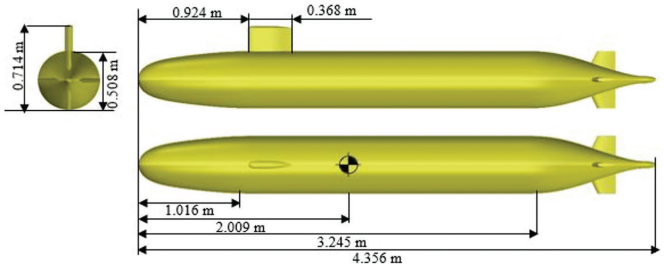

Figure 1. *DARPA Suboff AFF-8 configuration*

Table 1. *Main particulars of DARPA Suboff AFF-8*

L [m]	D [m]	H [m]	S [m²]	∇ [m³]	xg from FP [m]
4.356	0.508	0.714	6.348	0.706	2.009

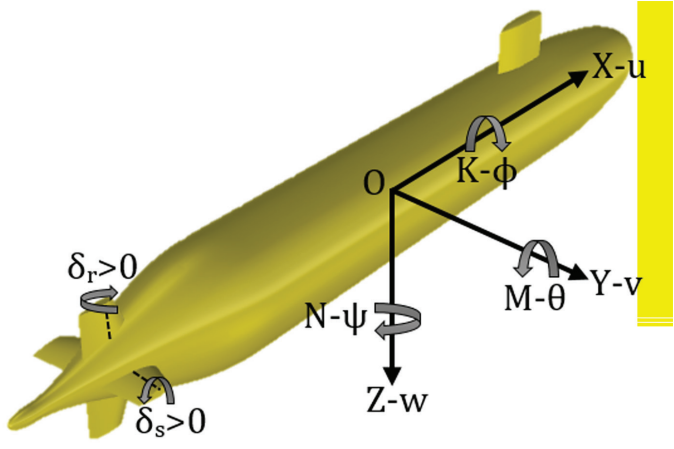

Figure 2. *The standard direction convention for motion parameters*

$$X', Y', Z' = \frac{X,Y,Z}{\frac{1}{2}\rho L^2 U^2}$$
$$K', M' N' = \frac{K,M,N}{\frac{1}{2}\rho L^3 U^2} \quad (1)$$

$$w', v', \delta_r, \delta_s = \alpha, -\beta, \delta_r, \delta_s \text{ (rad.)} \quad (2)$$

2.3. Equations of Motion

Together with the selected turbulence model equation(s); the continuity equation [Equation (3)] and the Unsteady Reynolds-Averaged Navier-Stokes Equations [Equation (4)] are governing the flow field,

$$\frac{\partial \overline{U}_i}{\partial x_i} = 0 \quad (3)$$

$$\frac{\partial \overline{U}_i}{\partial t} + \frac{\partial \overline{U_i U_j}}{\partial x_j} = -\frac{1}{\rho}\frac{\partial P}{\partial x_i} + \frac{\partial}{\partial x_j}\left\{\nu\left(\frac{\partial \overline{U}_i}{\partial x_j} + \frac{\partial \overline{U}_j}{\partial x_i}\right)\right\} - \frac{\partial U_i' U_j'}{\partial x_j} + f_i \quad (4)$$

Where mean velocity is denoted with $\overline{U}_i$, P represents the pressure, summation of the artificial viscosity due to turbulence modelling and molecular viscosity is represented by ν which is the effective viscosity. Density of the fluid is indicated with ρ and f_i represents the external momentum source in the "i" direction. Unsteady term of Equation (4) vanishes for the simulation cases not involving solid body motion. On contrary to the other simulation types, for RA simulations the momentum source term in Equation (4) is non-zero. Representing the steady rotational motion via MRF approach means the Coriolis force and the centrifugal acceleration expressed in Equation (5) acting on the UV.

$$MS = -\rho\left(2\Omega \times U_r + \Omega \times (\Omega \times r)\right) \quad (5)$$

Here, MS represents the momentum source, U_r is the relative velocity, Ω is the angular velocity and r represents the distance from rotation center. Because of change in rotation center, this source term needs to be modified as shown in Figure 3.

The components of the momentum source term with respect to rotation center A and rotation center B are demonstrated in Equation (6) and Equation (7), respectively.

$$MS_{xA} = -\rho\left(2\Omega \times U_r + \Omega \times (\Omega \times (x - x_A))\right)$$
$$MS_{yA} = -\rho\left(2\Omega \times U_r + \Omega \times (\Omega \times (y - y_A))\right) \quad (6)$$
$$MS_{zA} = -\rho\left(2\Omega \times U_r + \Omega \times (\Omega \times (z - z_A))\right)$$

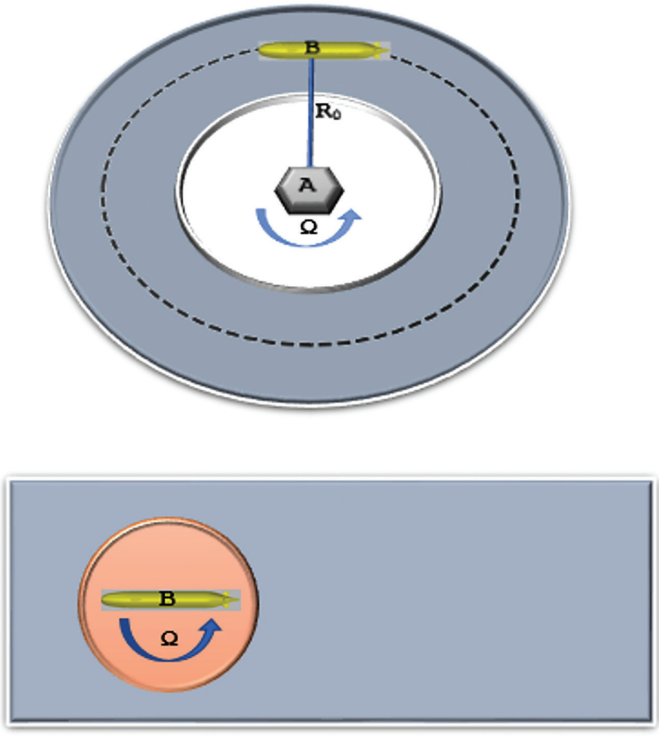

Figure 3. *Rotating reference frame vs. semi-relative reference frame domains*

$$\begin{aligned} MS_{xB} &= -\rho\left(2\Omega \times U_r + \Omega \times \left(\Omega \times (x - x_B)\right)\right) \\ MS_{yB} &= -\rho\left(2\Omega \times U_r + \Omega \times \left(\Omega \times (y - y_B)\right)\right) \\ MS_{zB} &= -\rho\left(2\Omega \times U_r + \Omega \times \left(\Omega \times (z - z_B)\right)\right) \end{aligned} \quad (7)$$

As can be observed in Figure 2; $x_B = x_A$, $|y_B - y_A| = R_0$ and $z_B = z_A$. The momentum source term in Equation (5) can be rexpressed as shown in Equation (8).

$$f_i = MS_{yA} - MS_{yB} = -\rho\Omega \times (\Omega \times R_0) \quad (8)$$

Reynolds Stress Term [i.e. $(\overline{U_i' U_j'})$] in the URANS equations is modelled using a two-equation turbulence model namely k-ω SST for closing the system of governing equations. Being an hybrid turbulence model, the k-ω SST turbulence model has high performance both in low and high Reynolds Number regimes of the flow. Additionally this turbulence model known to have good performance also with the separating flows.

2.4. Numerical Modelling

An overset structural grid, consisting of a rectangular prism background domain and a spherical overset domain, is used for all calculations. The mesh is generated using the native hexagonal mesh generation tool of OpenFOAM, known as snappyHexMesh, around the UV geometry. A combination of O-type and rectangular prism grid is used in overset domain, whereas background domain is consisting of only rectangular prism cells. Overset domain has a radius of 1.2 model length, and its center is arranged to coincide with the moment center of the UV. The background domain dimensions are chosen to be 17 L x 28 D x 28 D. Here, overall length of the model is represented with L, and "D" represents the maximum diameter of the model.

The meshing process consists of five steps: initially, a castellated mesh is generated for the overset domain. Cells are then deformed to snap the model geometry. Next an inflation layer is added adjacent to model surface. Afterwards a background mesh is generated. Merging of two mesh zones is the and final step. This results in a mesh with a total cell count of 24 million, which is used for all of the simulations under consideration. Perspective view of the domain grid and boundary conditions is presented in Figure 4.

Velocity inlet boundary condition is assigned to the front boundary. Where positive x axis is the direction of the velocity vector. Leeward boundary of the control volume is designated as pressure outlet. In order to assure parallel flow for the other boundaries which are positioned at an equal distance (i.e. 28 D) form the UV centerline, the symmetry boundary condition is applied.

All velocity components are enforced to be zero on model surface in order to satisfy the no-slip and no-penetration boundary conditions. Surface of the sphere enclosed the overset zone, is assigned to be an overset boundary. This boundary is used for exchanging information regarding primitive variables between two grids. High resolution spatial discretization is achieved in the low Reynolds number zone in close proximity of the UV. This is done for satisfying the requirement of dimensionless wall distance value of y+≈1 of the selected turbulence model. Non-dimensional wall distance distribution on the model surface is demonstrated in Figure 5.

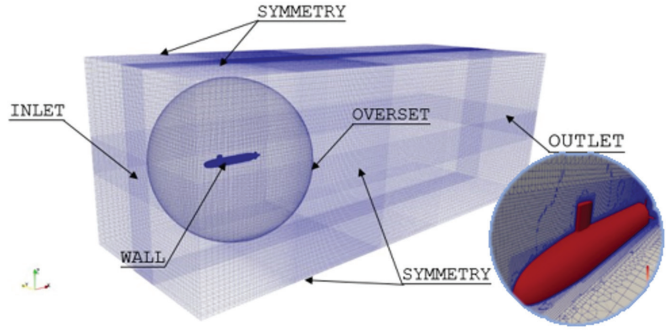

Figure 4. *Perspective view of the domain, grid and boundary conditions*

2.5. Simulation Matrix

Current part of the study involves the towing (straight and oblique) and steady turning simulations of the selected geometry. The simulation matrix of is demonstrated in Table 2. Steady-state simulations are carried out for the entire test matrix. Propulsive forces are not considered in the scope of this study.

3. Results and Discussion

3.1. Mesh Validation and Dependency

The mesh must be validated to ensure the production of accurate results. ITTC provide guidelines [28] for validation of the numerical marine hydrodynamics applications. Computational performance of the mesh is validated through commonly accepted quantities such as pressure and skin friction coefficients and resistance. In this study, validation is performed via a comparison of the above mentioned quantities. Table 3 and Figure 6 summarize the results. The agreement of the results with [29] is satisfactory. The maximum relative difference is less than 3%.

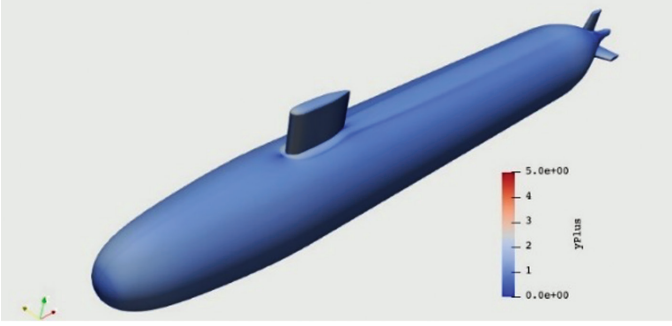

Figure 5. *y^+ Distribution on the surface*

Table 2. *Simulation matrix for the towing and steady turning motions*

Simulation type	U (ms^{-1})	Independent variable
Straight towing	3.046-9.255	3.046-9.255 for U (ms^{-1})
Oblique towing	3.00	-14° - +14° for α and β Δ β= Δ α=2°
Control surfaces	3.3436	-10° - +10° for δ_r and δ_s Δ δ_r = Δ δ_s = 5°
Rotational motion	3.00	10 – 16 m test radius R_0 Δ R=2 m

Table 3. *X-force comparison of the results with Liu and Huang [29]*

U	X-Force [N]		Diff.
[m/s]	CFD	DTRC	[%]
3.046	-105.12	-102.3	2.81
5.144	-278.5	-283.8	1.88
6.091	-382.3	-389.2	1.76
7.161	-516.6	-526.6	1.90
8.231	-670.3	-675.6	0.78
9.255	-835.0	-821.1	1.69

On the upper meridian line of the model; the pressure and skin friction coefficient distributions are measured for the same purpose. Skin friction coefficient (C_f) is presented in Figure 7. Benchmark data is provided by Qiu et al. [30]. Whereas large-eddy simulation (LES) results of Alin et al. [31] are used for benchmarking the pressure coefficient (C_p) distribution presented in Figure 8. Both distributions are in good agreement with the above mentioned benchmark data.

3.2. Oblique Towing

Figure 9 illustrates the variation in sway force (Y) roll (K) and yaw moment (N) with respect to drift angle (β) for drift angle interval of ±4°. Experimental benchmark data of (Zhao et al. [23]) also given for comparison. Coefficient of determination (R^2) is around unity for all three coefficient,

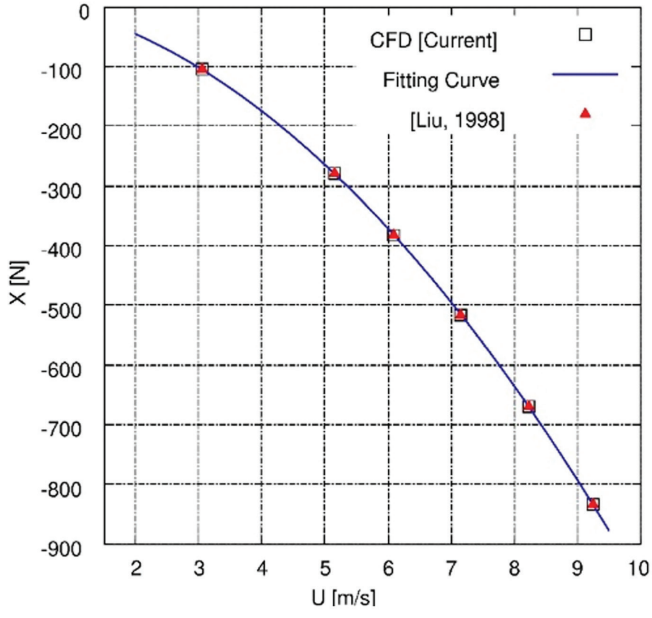

Figure 6. *X-force comparison of the results with Liu and Huang [29]*

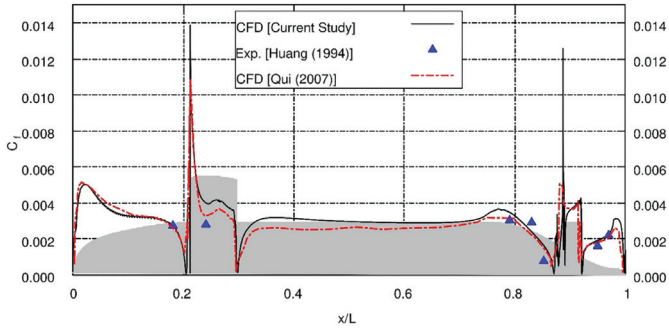

Figure 7. *C_f distribution on the upper meridian line of UV*

which means strong linearity in the data. The dimensionless coefficients of Y'_v, K'_v and N'_v are computed from the slope of the line fit. Results are presented and benchmarked in Table 4. Sway force (Y) and the yaw moment (N) data align well with the benchmark data and relative differences regarding the Y'_v, and N'_v are 6.52% and 0.15 respectively. As for the K'_v coefficient; relative difference is increased to 23%. This relatively high difference is due to limitation of the simulated motion to predict roll motion behavior of the vehicle. Hydrodynamic coefficients order associated with the roll motion known for being challenging to predict and generally requires advanced techniques such as conning motion [32].

In vertical plane; heave force (Z) and pitch moment (M) variation with respect to attack angle (α) are demonstrated in Figure 10 for attack angle interval of ±4°. Experimental benchmark data [23] also given for comparison. Coefficient of determination (R^2) is around unity for both of the coefficients which means strong linearity in the data. The dimensionless coefficients of Z'_w and M'_w are computed from the slope of the fitted line. Results are presented and benchmarked in Table 4. Heave force (Z) and pitch moment (M) data align well with the benchmark data and relative differences regarding the Z'_w and $M'_w$are 0.75% and 6.79 respectively.

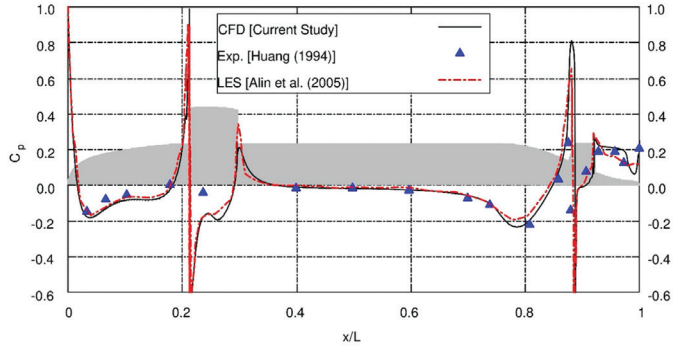

Figure 8. *C_p distribution on the upper meridian line of UV*

Table 4. *Tabulation of hydrodynamic coefficients*

Simulation type	Hydrodynamic coefficient	CFD	Benchmark	Ref	Diff. (%)
Straight towing	X'_{uu}	-0.00090	-0.0012	[24]	25.00
Oblique towing	Y'_v	-0.02925	-0.02746	[24]	6.52
	K'_v	-0.00058	-0.00047		23.40
	N'_v	-0.01375	-0.01377		0.15
	Z'_w	-0.01321	-0.01331		0.75
	M'_w	0.01029	0.01104		6.79
	X'_{vv}	0.01137	0.0130	[26]	12.54
	$Y'_{v\|v\|}$	-0.04932	-0.05775	[24]	14.60
	Z'_{vv}	0.08340	0.08474		1.58
	$K'_{v\|v\|}$	-0.00066	-0.00054		22.22
	M'_{vv}	0.01003	0.00951		5.47
	$N'_{v\|v\|}$	0.01264	0.01058		19.47
	X'_{ww}	0.0043	0.0065	[26]	35.50
	$Z'_{w\|w\|}$	-0.05410	-0.05193	[24]	4.18
	$Z'_{\|w\|}$	2.23-05	0.0000145		53.80
	Z'_{ww}	-0.001161	-0.000704		64.91
	$M'_{w\|w\|}$	0.000193	0.000143		34.96
	M'_{ww}	-0.00060	-0.00046		30.43

Table 4. *Continued*

Simulation type	Hydrodynamic coefficient	CFD	Benchmark	Ref	Diff. (%)
Steady rotational	Y'_r	0.004700	0.00499	[23]	5.81
	K'_r	-0.000110	-0.00013		15.38
	N'_r	-0.003700	-0.00408		9.73
	Z'_q	-0.00697	-0.00808		11.26
	M'_q	-0.00310	0.00392		20.91
	$Y'_{r\|r\|}$	-0.00396	-0.00422	[24]	6.16
	$N'_{r\|r\|}$	-0.0001961	-0.0001966		0.26
	$Z'_{q\|q\|}$	0.00274	0.00279		1.80
	$M'_{q\|q\|}$	0.000700	0.000838		16.47
Control surfaces	$Y'_{\delta r}$	0.0082	0.0069	[26]	19.40
	$N'_{\delta r}$	-0.0033	-0.0032		3.94
	$Z'_{\delta s}$	-0.0082	-0.0070		16.75
	$M'_{\delta s}$	-0.0033	-0.0032		3.30
	$X'_{\delta r\delta r}$	-0.0041	-0.0042		2.38
	$X'_{\delta s\delta s}$	-0.0025	-0.0030		16.67
	$K'_{\delta r}$	2.66E-06	5.00E-6	[25]	46.90
*Table 4 includes two columns					

Variations of forces and moments in 6-DOF with respect to drift angle (β) are demonstrated in Figure 11. Drift angle range is selected as ±14° (with an increment of 2°) in order to observe the non-linear changing behavior of forces and moments. Results of X and Z force as well as M moment are represented with a quadratic curve fit. Whereas Y force K and M moment results are represented with a 3rd degree polynomial. Excluding the Z force and M moment variation R^2 values are around one which means fitted curves can successfully represent the data. Computed coefficients of X'_{vv}, $Y'_{v|v|}$, Z'_{vv} $K'_{v|v|}$, M'_{vv} and $N'_{v|v|}$ from this data is presented and benchmarked in Table 4. If the variation of force/moment is represented by a quadratic curve, the resulting coefficient is the coefficient of the quadratic term. Taylor series expansion is not included terms like$Y'_{v|v|}$. Their inclusion is motivated by physical arguments [33]. For variations represented by a 3rd polynomial, definition of the associated hydrodynamic coefficient is as; $Y'_{v|v|} = \partial^2 Y/\partial|v|\partial v$ at $v = 0$.

The coefficient of X'_{uu} is obtained from the quadratic curve fitted to the data demonstrated in Figure 6. The resulting coefficient deviates from the benchmark data [24] by 25%. This difference is caused by the difference in accuracy level of drag predictions. Current study has a maximal difference of 3% as can be seen in Table 3 compared to 7% relative difference declared by Zhao et al. [23].

Similarly non-linear variations of X and Z force as well as M moment with respect to angle of attack (α) is presented in Figure 12 for the angle of attack range of ±14° (with an increment of 2°). Results of X force as well as M moment are represented with a quadratic curve fit. Whereas Z force results are represented with a 3rd degree polynomial. R^2 values are around one which means fitted curves can successfully represent the data. Computed coefficients of X'_{ww}, $Z'_{w|w|}$, $Z'_{|w|}$, Z'_{ww}, M'_w $M'_{w|w|}$ and M'_{ww} from this data is presented and benchmarked in Table 4.

3.3. Steady Rotational Motion

Sway force, roll and yaw moment variations with respect to yaw angular velocity (r=0.1875~0.3 rad s^{-1}) are demonstrated in Figure 13 for R_0=10 ~16 m. The dimensionless coefficients

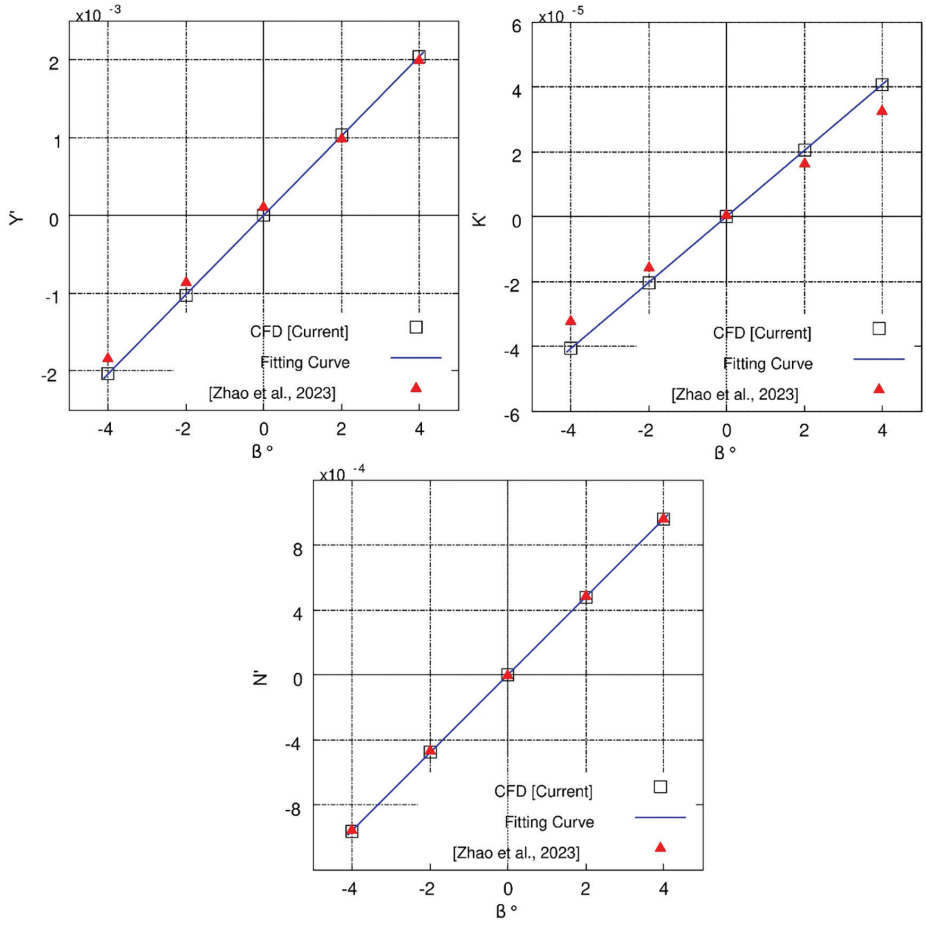

Figure 9. *Oblique towing simulation results in the linear range (horizontal plane)*

**Figure 9 includes two columns*

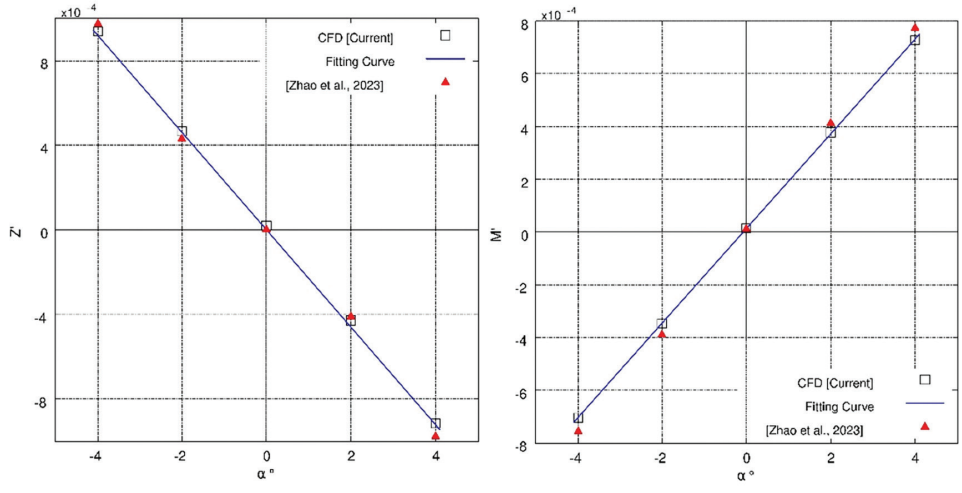

Figure 10. *Oblique towing simulation results in the linear range (vertical plane)*

**Figure 10 includes two columns*

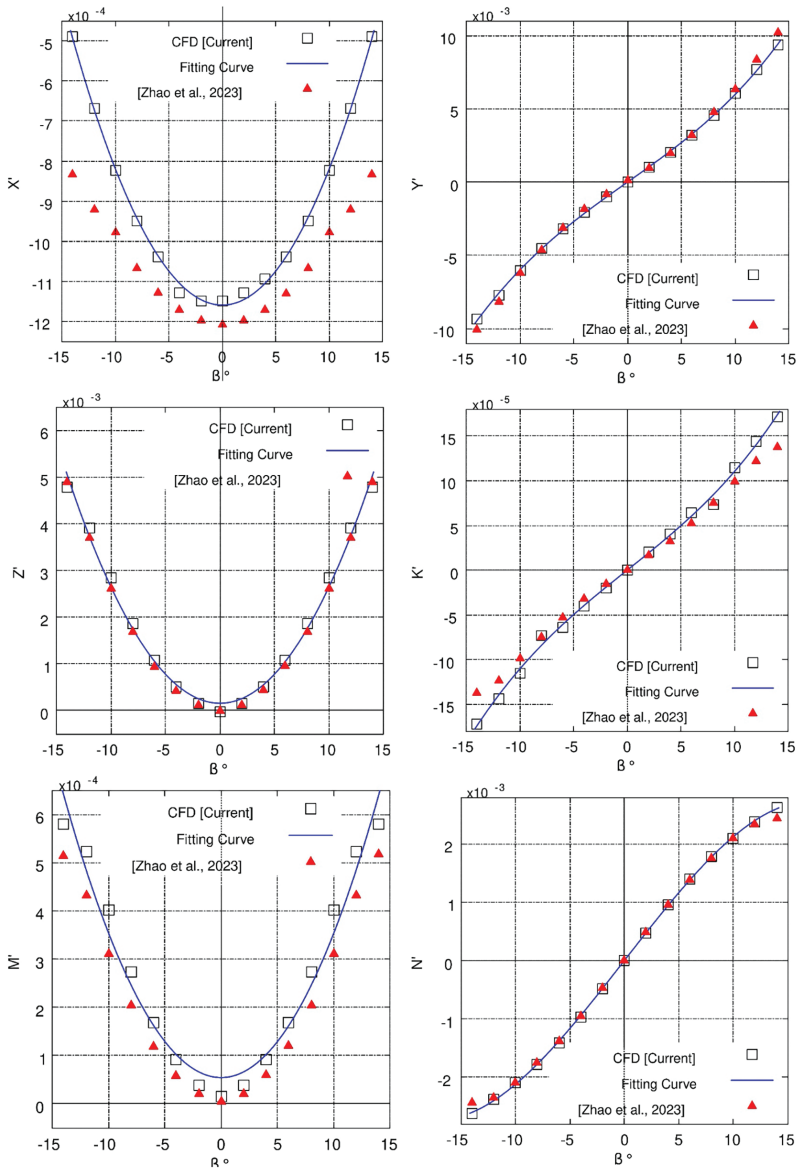

Figure 11. *Oblique towing simulation results in the non-linear range (horizontal plane)*

**Figure 11 includes two columns*

of Y'_r, K'_r and $N'_r$are computed from linear regression. Results are presented and benchmarked in Table 4 In general utilized method for simulation of the steady rotational motion fall short of predicting sway force and yaw moment for the entire test cases. The difference is 35% in average which is associated with two particular reasons. First of all, multiple reference frame (MRF) approach known its severe effects on the flow field and under prediction of the forces and moments. Second reason is originated from the effect of Vortex Induced Vibrations created by the cylindrical strut used in the experiments [23,24]. However MRF method demonstrates a good performance in predicting the rate of change of forces and moments with respect to dimensionless rotation radius where r'=L/R.

For roll moment predictions harmony between simulations and experimental results are quite satisfactory. This phenomenon is also observed by Kim et al. [34] for the rotation motion simulation of bare hull DARPA Suboff modeled via MRF. Y'_r and N'_r are predicted in a 10% relative difference range. Relative difference associated with the prediction of N'_r is slightly greater than the Y'_r. K'_r coefficient is an order of magnitude smaller than the other measured quantities during the simulations. This means steady rotational motion creates very small roll moment due to

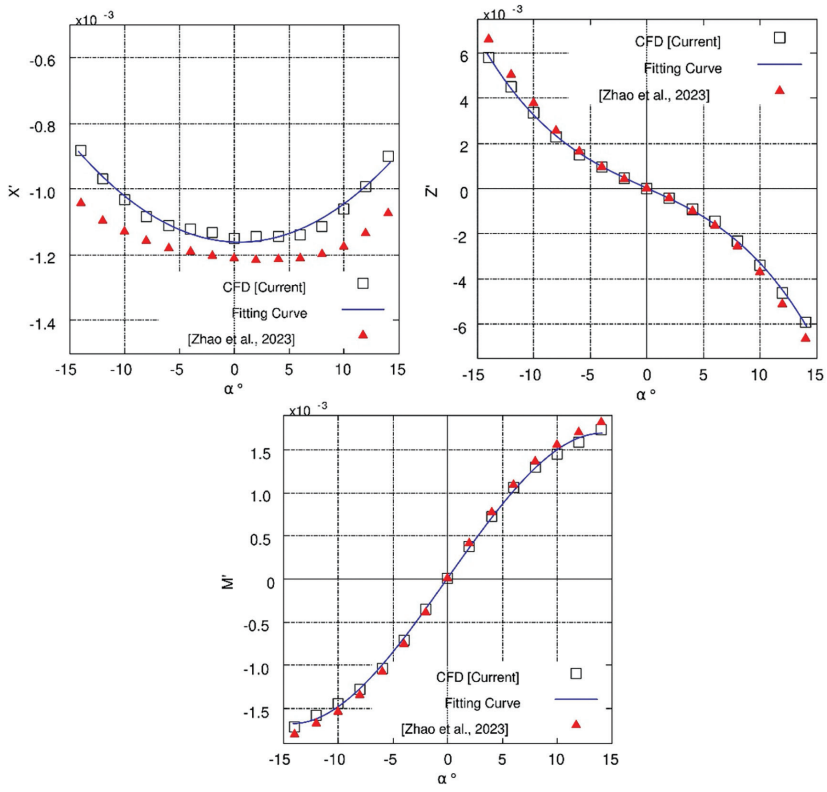

Figure 12. *Oblique towing simulation results in the non-linear range (vertical plane)*

**Figure 12 includes two columns*

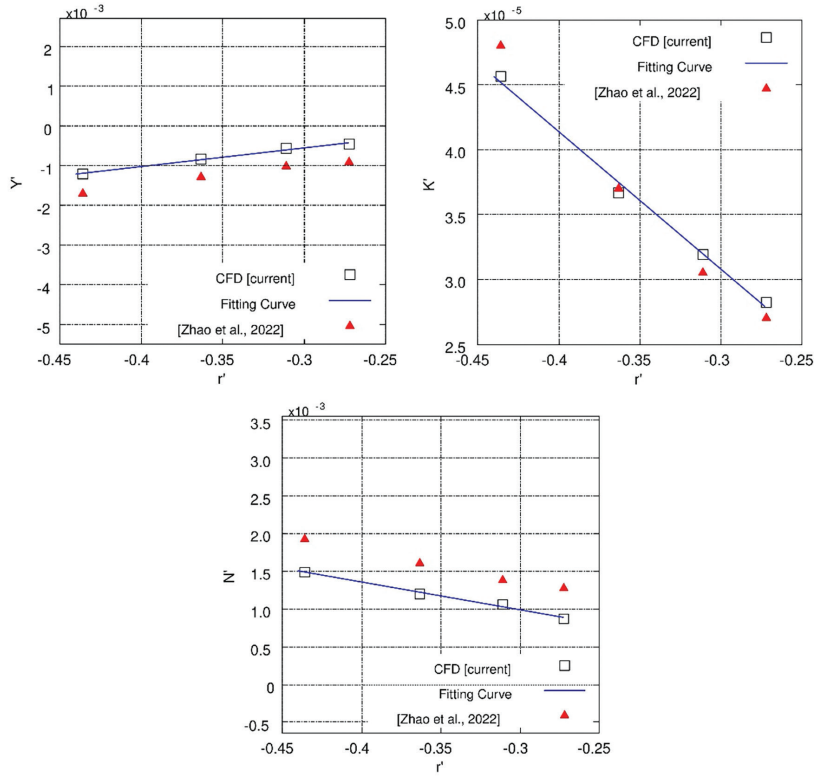

Figure 13. *Steady rotational motion simulation results at 0° incidence (horizontal plane)*

**Figure 13 includes two columns*

the geometric characteristics of the UV. It is hard to achieve an accuracy level for K'_r similar to the other dimensionless quantities. The relative difference associated with the K'_r coefficient is around 15%. The coefficients $Y'_{r|r|}$ and $N'_{r|r|}$ are derived directly from the quadratic curve fitted to the data. The maximum relative difference is 6 % as can be seen in Table 4.

Data related with the steady rotational motion has also noise as in the experiments. Simulations are continued at least 500 additional pseudo time steps after reaching the established convergence criteria of 10^{-5} for primitive variables and turbulence quantities. An oscillatory convergence behavior is observed and the results of integral quantities seems to have small oscillations around an average value.

Steady rotational motion in vertical plane is investigated through its effects on the heave force (Z) and pitch moment (M). Their variation with respect to pitch angular velocity (q=0.1875~0.3 rad/s) are demonstrated in Figure 14 for R_0=10 ~16 m. (with an increment of 2 m). The dimensionless coefficients of Z'_q and M'_q are computed from linear regression. Results are presented and benchmarked in Table 4. As in case of the steady turning motion in horizontal plane; heave force and pitch moment are also under predicted by MRF algorithm. Nevertheless rate of change of heave force and pitch moment with respect to dimensionless rotation radius where q'=L/R can be predicted sufficiently accurate.

Corresponding hydrodynamic coefficients of Z'_q and M'_q are predicted in a 20% difference range. Relative difference associated with the prediction of M'_q is slightly greater than the Z'_q. The coefficients of $Z'_{q|q|}$ and $M'_{q|q|}$ are derived directly from the quadratic curve fitted to the data. The maximum relative difference is around 16%.

3.4. Control Surface Deflection

Variations in surge (X) and sway force (Y) as well as roll (K) and yaw moment (N) as a result of rudder deflection (δ_r) are demonstrated in Figure 15 for rudder angle interval of ±10° (with increment of 5°). Experimental results of Khan et al. [26] and Roddy [25] (in case of roll moment) are also plotted along with the simulation data for comparison purpose. All four quantities exhibit a variation trend which is aligned with the above mentioned benchmark data. Variations of sway force (Y), roll moment (K) and yaw moment (N) are represented with a line fit. On the other hand surge force (X) variation displays quadratic behavior. Computed coefficients of $Y'_{\delta r}$, $K'_{\delta r}$, $N'_{\delta r}$ and $X'_{\delta r\delta r}$ from these regressional analyses are presented and benchmarked in Table 4. Excluding the hydrodynamic coefficient of $K'_{\delta r}$ the maximum relative difference with respect to experimental benchmark data is around 19%. For $K'_{\delta r}$ a relative difference of 47% is calculated. Deviation in this coefficient is attributed to the above mentioned challenges of accurately capturing roll motion behavior for UVs.

In vertical plane elevator deflection is effective on the surge (X) and heave (Z) forces and pitch moment (M). Variations in these quantities with respect to elevator deflection is presented along with the experimental results [26] in Figure 16 for elevator angle interval of ±10° (with increment of 5°). All four quantities exhibit a variation trend which is aligned with the above mentioned benchmark data. Variations of heave force (Z), pitch moment (M) are represented with a line fit whereas surge force (X) variation can be expressed with a quadratic curve. Computed coefficients of $Z'_{\delta s}$, $M_{\delta s}$ and $X'_{\delta s\delta s}$ based on the results of these regression analyses are presented and benchmarked in Table 4. The maximum relative difference is under 17 % for these coefficients.

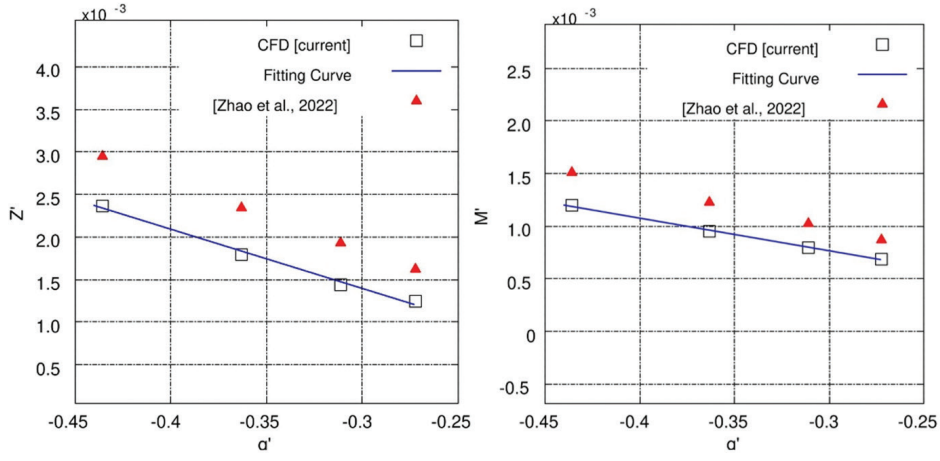

Figure 14. *Steady rotational motion simulation results at 0° incidence (vertical plane)*

**Figure 14 includes two columns*

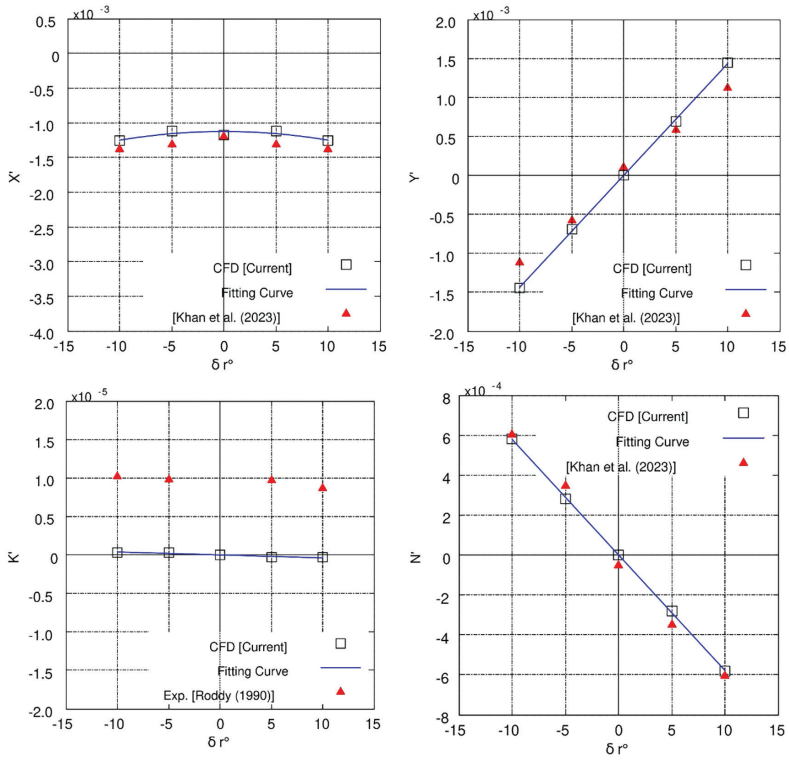

Figure 15. *Control surface simulation results (Rudder)*

**Figure 15 includes two columns*

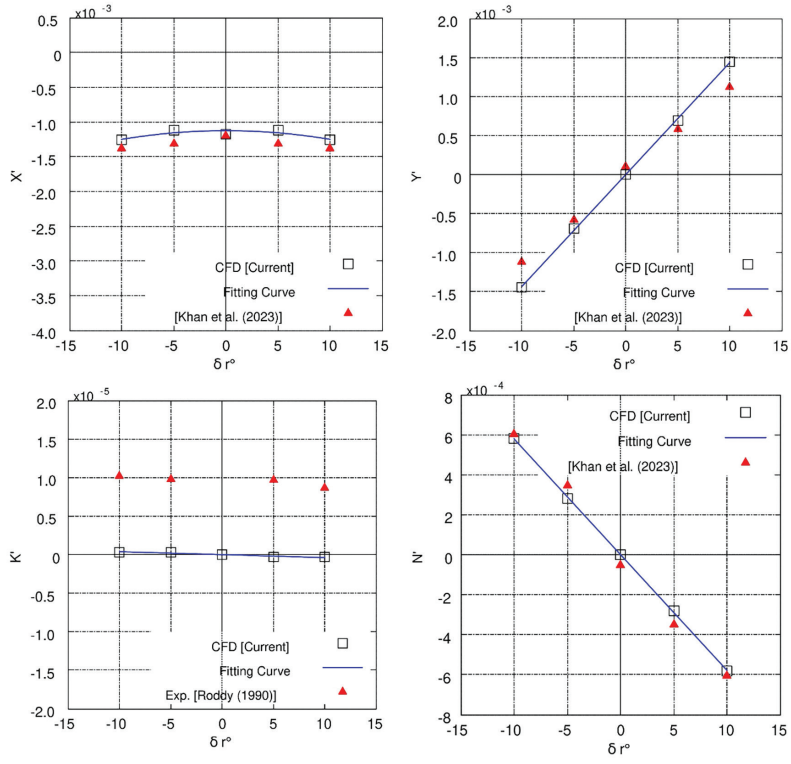

Figure 16. *Control surface simulation results (Elevator)*

**Figure 16 includes two columns*

3.5. Summary and Discussion

Time-independent hydrodynamic coefficients of fully appended DARPA Suboff configuration (AFF-8) are computed, presented and benchmarked in Table 4. For each coefficient reference for the benchmark value is also given. Overall comparable results with the benchmark data are obtained from the numerical analyses. Deviation in the roll moment coefficients is attributed to the inability of the simulated motion to predict roll motion response of the vehicle

For the nonlinear coefficients of the heave force with respect to heave velocity; probable cause of the deviations from the benchmark data is extreme non-linearity due to the existence of sail. As the angle of attack increased, flow field becomes more and more non-linear. Between simulations and experiments it is very challenging to achieve a harmony in the results due to these non-linear effects.

4. Conclusion

A methodology is proposed in this paper for mimicking the motions of the main experimental facilities by using the same grid structure. Independent variable (i.e. drift/attack/control surface deflection angle and rotation radius) intervals, which corresponds to the linear and non-linear variations of dependent variables (i.e. force and moments) are investigated. An extensive set of hydrodynamic coefficients of fully appended DARPA Suboff configuration (AFF-8) associated with the straight/oblique towing and steady turning motions are computed and benchmarked.

The subsequent findings can be outlined as follows:

• Hydrodynamic coefficients of 1st associated with the linear velocities are predicted with a desired level of accuracy. Except roll moment variation with respect to sway velocity. This is attributed to the challenges of capturing roll motion behaviour of the UV with oblique flow simulations.

• In horizontal plane; hydrodynamic coefficients of 2nd order are also well predicted. However in vertical plane, due to the asymmetry of the vehicle, non-linearities become dominant as the angle of attack increased. As a result achieving a harmony between simulations and experiments becomes very challenging. This phenomena can be observed in Table 4.

• Although forces and moments are under predicted by MRF algorithm in steady turning motion, 1st order hydrodynamic coefficients of angular velocities is generally well predicted.

• For 2nd order hydrodynamic coefficients of angular velocities harmony between the simulation results and the benchmark data is satisfactory.

• In general control surface coefficients both in first and second order are aligned with the benchmark experimental data except for the roll motion coefficient with respect to rudder angle. Deviation in this coefficient with respect to experiments is again due to the challenges of capturing roll motion behaviour of the UV.

Overall, this study contributes to the literature by offering a robust methodology for simulating the motions associated with major experimental setups by reducing the amount of pre-processing work significantly. This is achieved by the modification of governing equations which requires a deep understanding of the mathematics behind the solution algorithms and the software structure. The methodology used in the paper and findings provide comprehensive and insights for researchers in the field of marine hydrodynamics for changing their perspective on the maneuvering problem..

Authorship Contributions

Concept design: O. Kırıkbaş, and Ş. Bal, Data Collection or Processing: O. Kırıkbaş, Analysis or Interpretation: O. Kırıkbaş, and Ş. Bal, Literature Review: O. Kırıkbaş, Writing, Reviewing and Editing: O. Kırıkbaş, and Ş. Bal.

Funding: The authors did not receive any financial support for the research, authorship and /or publication of this article.

References

[1] M. Gertler, and G. Hagen, *Standard Equations of Motion for Submarine Simulation.* Technical Report AD653861, June, 1967.

[2] J. Feldman, *DTNSRDC Revised Standard Submarine Equations of Motion.* David Taylor Research Center, Ship Performance Department (June), 1979.

[3] J. A. Foroushani, and M. Sabzpooshani, "Determination of hydrodynamic derivatives of an ocean vehicle using CFD analyses of synthetic standard dynamic tests." *Applied Ocean Research,* vol. 108, 102539, Mar 2021.

[4] B. Overpelt, B. Nienhaus, and B. Anderson, "Free running manoeuvring model tests on a modern generic SSK class submarine (BB2)", *Pacific International Maritime Conference*, 2015.

[5] P. M. Carrica, M. Kerkvliet, F. Quadvlieg, M. Pontarelli, and J. E. Martin, CFD Simulations and Experiments of a Maneuvering Generic Submarine and Prognosis for Simulation of Near Surface Operation, 31st Symposium on Naval Hydrodynamics Monterey, CA, USA, 2016.

[6] G. Dubbioso, R. Broglia, and S. Zaghi, "CFD analysis of turning abilities of a submarine model". *Ocean Engineering,* vol. 129, pp. 459-479, Jan 2017.

[7] H. Kim, D. Ranmuthugala, Z. Q. Leong, and C. Chin, "Six-DOF simulations of an underwater vehicle undergoing straight line and steady turning manoeuvres". *Ocean Engineering,* vol. 150, pp. 102-112, Feb 2018.

[8] Y.x. Wang, J.-f. Liu, T.-j. Liu, Z.-b. Jiang, Y.-g. Tang, and C. Huang, "A numerical and experimental study on the hull-propeller interaction of a long range autonomous underwater vehicle". *China Ocean Engineerin*g, vol. 33, pp. 573-582, Oct 2019.

[9] C. Delen, and O. K. Kinaci, "Direct CFD simulations of standard maneuvering tests for DARPA Suboff". *Ocean Engineering,* vol. 276, pp. 114202, May 2023.

[10] O. Kırıkbaş and Ş. Bal, "Simulation of captive model experiments of an underwater vehicle by CFD based on a single grid structure". In *4th International Symposium on Naval Architecture and Maritime (INT-NAM 2023)*, Istanbul, Turkey, pp. 947-960, Oct 2023.

[11] O. Kırıkbaş and Ş. Bal, *DELOK'23 Calculation of Maneuvering Coefficients of an Underwater Vehicle in CFD Environment Based on the Same Grid Topology,* I. International Maritime and Logistics Congress (MARLOG 2023, Hybrid), Zonguldak Bülent Ecevit University, Maritime Faculty, Zonguldak, Türkiye, September 22-23, 2023, pp. 248-262.

[12] A. Phillips, M. Furlong, and S. Turnock, "Virtual planar motion mechanism tests of the autonomous underwater vehicle autosub," *in STGConference/Lectureday: CFD in Ship Design*, 2007.

[13] H. Zhang, Y. R. Xu, and H. P. Cai, "Using CFD software to calculate hydrodynamic coefficients". *Journal of Marine Science and Application,* vol. 9, pp. 149-155, Jun 2010.

[14] Y. Pan, H. Zhang, and Q. Zhou, "Numerical prediction of submarine hydrodynamic coefficients using CFD simulation". *Journal of Hydrodynamics,* vol. 24, pp. 840-847, Dec 2012.

[15] D. E. Humphreys, and K. W. Watkinson, "*Prediction of acceleration hydrodynamic coefficients for underwater vehicles from geometric parameters".* Naval Coastal Systems Laboratory, Panama City, Florida, 1978.

[16] Z. Lin, and S. Liao, "Calculation of added mass coefficients of 3D complicated underwater bodies by FMBEM". *Communications in Nonlinear Science and Numerical Simulation,* vol. 16, pp. 187-194, 2011.

[17] E. Javanmard, S. Mansoorzadeh, and J. A. Mehr, "A new CFD method for determination of translational added mass coefficients of an underwater vehicle". *Ocean Engineering,* vol. 215, 107857, Nov 2020.

[18] O. Kırıkbaş, and Ş. Bal, "Computation of added mass coefficients of darpa suboff using two different solvers of OpenFOAM", International Conference on Postgraduate Research in Maritime Technology (PostGradMarTech 2023), Hellenic Institute of Maritime Technology (HIMT) Athens, Greece, 8-9 Nov 2023.

[19] S. Toxopeus, "Viscous-flow calculations for bare hull DARPA SUBOFF submarine at incidence". *International Shipbuilding Progress,* vol. 55, pp. 227-251, 2008.

[20] A. Phillips, M. Furlong, and S. R. Turnock, *The use of computational fluid dynamics to determine the dynamic stability of an autonomous underwater vehicle, 10th numerical towing tank symposium (NuTTS'07),* Hamburg, Germany, 2007.

[21] L. Cao, J. Zhu, and G. Zeng, "Viscous-flow calculations of submarine maneuvering hydrodynamic coefficients and flow field based on same grid topology". *Journal of Applied Fluid Mechanics,* vol. 9, pp. 817-826, Feb 2016.

[22] W. Xiaocui, W. Yiwei, W. Chenguang, H. Zhiqiang, and Y. Ruiwen, "An effective CFD approach for marine-vehicle maneuvering simulation based on the hybrid reference frames method". *Ocean Engineering,* vol. 109, pp. 83-92, Nov 2015.

[23] B. Zhao, et al. "Hydrodynamic coefficients of the DARPA SUBOFF AFF-8 in rotating arm maneuver: Part I: Test technology and validation". *Ocean Engineering,* vol. 266, 113148, 2022.

[24] B. Zhao, Y. Yun, F. Hu, J. Sun, D. Wu, and B. Huang, "Hydrodynamic coefficients of the DARPA SUBOFF AFF-8 in rotating arm maneuver - Part II: Test results and discussion." *Ocean Engineering,* vol. 268, 113466, Jan 2023.

[25] R. F. Roddy, *Investigation of the stability and control characteristics of several configurations of the DARPA suboff model (DTRC Model 5470) from captive-model experiments.* David Taylor Research Center, Departmental Report DTRC/SHD- 1298- 08 (September), 1990.

[26] M. K. Khan, M. Korulla, V. Nagarajan, and O. P. Sha, "Measurements of steady manoeuvring forces and moments over an axisymmetric body with appendages in a wind tunnel". *Ship Technology Research*, pp. 1-12, Dec 2023.

[27] N. C. Groves, T. T. Huang, and M. S. Chang, *"Geometric characteristics of DARPA Suboff models: (DTRC Model Nos. 5470 and 5471)*". David Taylor Research Center, 1989.

[28] ITTC, 2011. CFD, General CFD Verification, in ITTC - Recommended Procedures and Guidelines.

[29] H. Liu, and T. T. Huang, "Summary of DARPA suboff experimental program data" Naval Surface Warfare Center Carderock Division (NSWCCD), West Bethesda, MD, USA, Report No. CRDKNSWC/HD-1298-11, 1998.

[30] L. Y. Qiu, Z. K. Shi, G. X. Hou, and F. F. Wei, "Validation of numerical simulation of the flow over submarine geometries with full appendages". *Journal of Ship Mechanics*, vol. 11, pp. 341-350, Jun 2007.

[31] N. Alin, et al. "3D unsteady computations for submarine-like bodies". In *43rd AIAA Aerospace Sciences Meeting and Exhibit,* Jan 2005.

[32] J. Y. Park, et al. "Study on coning motion test for submerged body". *Journal of Ocean Engineering and Technology,* vol. 29, pp. 436-444, Dec 2015.

[33] M. S. Triantafyllou, and F. S. Hover, *Maneuvering and control of surface and underwater vehicles*, 2004, [Online].

[34] T. W. Kim, T. J. Kang, W. G. Park, and C. M. Jung, "Estimation of roll coefficient of underwater vehicle using a calculation of hydrodynamic forces". *Journal of Computational Fluids Engineering,* vol. 20, pp. 81-87, Jun 2015.